Heliyon 10 (2024) e33396

Contents lists available at ScienceDirect

Heliyon

journal homepage: www.cell.com/heliyon

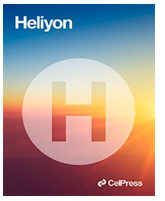

Research article

Synthesis and characterization of magnetic molecularly imprinted polymers for the rapid and selective determination of clofazimine in blood plasma samples

Nur Masyithah Zamruddin [a,b], Herman Herman [b], Saliza Asman [c], Aliya Nur Hasanah [a,d,*]

[a] Department of Pharmaceutical Analysis and Medicinal Chemistry, Faculty of Pharmacy, Universitas Padjadjaran, Jl. Raya Bandung Sumedang KM 21, Sumedang, 45363, Indonesia
[b] Department of Pharmaceutical Chemistry, Faculty of Pharmacy, Mulawarman University Gunung Kelua, 75119 Indonesia
[c] Department of Physics and Chemistry, Faculty of Applied Sciences and Technology, Universiti Tun Hussein Onn Malaysia, UTHM Pagoh Campus, Pagoh Higher Education Hub, KM 1, Jalan Panchor, 84600, Muar, Johor, Malaysia
[d] Drug Development Study Center, Faculty of Pharmacy, Padjadjaran University, Jl. Raya Bandung Sumedang KM 21, Sumedang, 45363, Indonesia

ARTICLE INFO

Keywords:
Magnetic molecular imprinted polymer
Solid phase extraction
Clofazimine

ABSTRACT

Clofazimine (CLF) is a riminophenazine derivative and a new therapeutic option with high efficacy for patients with rifampicin-resistant tuberculosis (TB). The blood levels of CLF are low and suboptimal, so therapeutic drug monitoring is required. Prior to this study, there were no molecular imprinting–based solid phase extraction (SPE) sorbents that could be used to determine the blood CLF levels. Hence, we prepared a magnetic molecularly imprinted polymer (MMIPs) to capture CLF. We employed computational selection of a functional monomer and crosslinker and confirmed these selections based on the association constant (K_a) and a Job plot. We synthesised MMIPs with two surface modifiers and characterized the polymers. Our computational analysis based on the bond energy revealed that methyl methacrylate (MMA) was the most suitable functional monomer at a CLF-to-MMA molar ratio of 1:4. Based on the bond energy, the most suitable crosslinker was trimethylolpropane trimethacrylate (TRIM) at a CLF-to-TRIM molar ratio of 1:1. We determined the K_a of MMA and TRIM in different solvents. Isopropanol produced the highest K_a. The Job plot showed that a template-to-MMA-to-TRIM molar ratio of 1:4:20 was optimal to synthesize imprinted polymer in isopropanol. We prepared MMIPs using two different modifiers, namely aminopropyltrimethoxysilane (APTES) and oleic acid (OA), using the ratio determined from the Job plot. Physical characteristic tests carried out using FT-IR, SEM-EDS, PSA, BET and VSM, showed that the synthesis was success with a spherical and uniform agglomeration of particles, also a flat surface with many holes with a particle size of MMIP-APTES and MMIP-OA respectively 0.14 μm and 0.28 μm, showed a surface area for MMIP-APTES is 2874.51 m^2/g and MMIP-OA 2913.07 m^2/g, exhibiting superparamagnetic properties with a saturation magnetization value of MMIP-APTES 21.1 emu/g^{-1} and MMIP-OA 49.9 emu/g^{-1}. Adsorption capacity result showed that MMIP-OA fits well with the Langmuir model, while MMIP-APTES fits better with the Freundlich. Application of MMIP-SPE (Magnetic Molecular Imprinted Polymer-Solid Phase Extraction) APTES resulted 92.3 ± 6.1 % and MMIP-SPE-OA 51.5 ± 8.1 % for

* Corresponding author. Department of Pharmaceutical Analysis and Medicinal Chemistry, Faculty of Pharmacy, Universitas Padjadjaran, Jl. Raya Bandung Sumedang KM 21, Sumedang, 45363, Indonesia
E-mail addresses: nur21050@mail.unpad.ac.id (N.M. Zamruddin), aliya.n.hasanah@unpad.ac.id (A.N. Hasanah).

https://doi.org/10.1016/j.heliyon.2024.e33396
Received 4 January 2024; Received in revised form 19 June 2024; Accepted 20 June 2024
Available online 26 June 2024

recovering CLF in blood. The result of selectivity test also showed that MMIP-SPE-APTES is better than MMIP-SPE-OA and selectively recover CLF from human blood plasma existed together with other TB-Drugs. The study result shows that MMIPs with APTES modification can be used for CLF determination in human blood plasma.

1. Introduction

Clofazimine, a derivative of riminophenazine, shows inhibition against Mycobacterium tuberculosis in vitro and in vivo. In 2010, clofazimine began to be used to treat TB because cases of drug resistance *M.Tuberculosis* began to spread. Clofazimine used as second-line compound for used in combination with other drug in the treatment of multidrug-resistant TB (MDR-TB, defined as resistance to at least isoniazid and rifampicin) on 2019 by WHO as it can shortening the duration of treatment [1,2].CLF is highly protein bound and accumulates in macrophages and fat; thus, it has a very long half-life (70 days) increases the risk of side effects and the emergence of resistance due to decreased patient compliance and suboptimal blood levels [3,4]. Hence, therapeutic drug monitoring in patients with MDR-TB is crucial to ensure adequate and optimal levels of absorbed drugs in the body [5,6]. Due to the low serum levels, sensitive analytical methods are required to detect CLF [7–9]. The lowest concentration of CLF is < 48 ng/ml [10]. The analytical method used to determine CLF levels to date has been carried out by Machado et al. [11]. Analysis of clofazimine determination using the Chromatographic method of clofazimine in nanoformulation showed recovery of $\geq$86.2 %. Other method carried out by Du Preez et al. [12] used HPLC to analyze simultaneously artemisone, clofazimine and decoquinate showed recovery for clofazimine of 99 %. In this research, we will develop a method for analyzing clofazimine using magnetic solid phase extraction [13] that never been done by others, where the polymer is designed with the addition of clofazimine as a template for analysis of human blood samples.

The molecular imprinted polymer (MIP) technique is a molecular imprinting method using target molecules (drug compounds or other analytes) in the form of a synthetic polymer matrix that can bind target molecules selectively [14]. The conventional method commonly used for the isolation of various analytes is solid phase extraction (SPE), which is a reliable and cost-effective technique for the selective isolation and concentration of various analytes and sample matrices [15]. The latest generation of MIPs involves the design and use of specific molecular recognition agents capable of mimicking the properties of natural recognition sites due to imprinting [16]. The polymer will have artificial recognition sites for the target molecule and its analogues [14]. MIP has been developed and used for sample preparation; it is selective and has a high recovery values [17]. As explained above, CLF requires a sensitive analysis method because the levels in blood serum are low. MIP can be used as a specific extraction method for CLF in blood samples. CLF is a strong base that has one hydrogen bond donor group and four hydrogen bond acceptor groups (PubChem). Thus, monomers with hydrogen bond donor or acceptor groups can be selected to form molecular recognition sites. MIPs made using the commonly used bulk polymerisation method have several weaknesses, including heterogeneous and irregular polymer shapes, in addition, the adsorption site on bulk polymers is too far from the surface, so the binding capacity of target ions is poor [18]. To overcome these problems, a MIP can fabricated on the surface of a magnetic substrate to generate a magnetic molecularly imprinted polymer (MMIP). This design allows magnetic separation [13]. There have been various modifications and iterations of SPE among which Karrat et al. [19] developed a new strategy incorporating magnetic molecularly imprinted polymer (MMIP) as an artificial antibody and confirmed the success of MMIP preparation. MMIP was synthesised through a radical polymerisation process and showed good average recovery results between 92.2 % and 104.7 %. Giebułtowicz et al. [20] has developed a magnetic molecularly imprinted nano-conjugate sorbent for effective dispersive solid phase extraction of antazoline (ANT) and its metabolite, hydroxyantazoline (ANT-OH) showing pharmacokinetic results that the new sorbent can be useful in the extraction of ANT and ANT-OH from human plasma. As also done by Sobiech et al. [21], they developed and validated a new analytical method to determine the pharmacokinetic profile hordenine in plasma samples with Magnetic Core−Shell Imprinted Nanoconjugates sorbents in the presence of magnets facilitates the pretreatment step with highly complex samples, thereby reducing time and costs. demonstrated the determined pharmacokinetic profile of hordenine. Malik et al. [22] have also developed a magnetic molecularly imprinted polymer-based electrochemical sensor for dye quantification, showing the imprinted polymer has higher detection capability and selectivity towards SY dyes as an electrochemical sensors compared to non-imprinted polymers. Research conducted by Wu et al. [23] has also developed quercetin molecular imprinted polymer using cellulose as a carrier (CMMs@MPS@MIPs), porous cellulose microspheres (CMMs) were successfully prepared with cotton as the raw material, and MIPs grafted after silanization modification showed selectivity values which is high for quercetin. MMIP has the advantage of fast and effective binding to the template used. Physically, MMIP has a spherical polymer shape and the advantage of MMIP is that it is a sorbent that has magnetic properties, other properties are that it has high selectivity to the template and it can be easily isolated from samples with a magnet. This last advantage means that external filtration or centrifugation steps are not required, pre-treatment times are shorter and there is reversible and controlled flocculation [24–26].

Based on our search of mipdatabase.com, there are no MMIP-SPE sorbents for CLF. To achieve higher mass transfer and overcome the shortcoming of bulk MIP production, we prepared MMIP for CLF and then modified the surface with aminopropyltrimethoxysilane (APTES) or oleic acid (OA). OA as the organic anion chelator is commonly used to coated the Fe_3O_4 as it can makes the surface of polymer molecules amphoteric, which increases solubility in polar solutions (for example in water) [13]. Modification of the surface using APTES also done as the comparison as APTES is widely used because of its ability to bind to different functional groups and can provide a SiO_2 layer [27]. The wide application capability of siloxane is due to its good properties, namely flexible, elastic, strong, resistant to physical and chemical factors, stable to heat and strong to pressure [28]. Research conducted by Lafarge et al. [29] sol–gel

molecularly imprinted silica (MIS) for fungicide using (3-Aminopropyl) trimethoxysilane showed higher imprinting factor 135 times higher than MIP without silica modification due to more chemically stable and specific toward the target species. In order to synthesize the Magnetic Molecularly Imprinted Polymers for CLF, we employed computational analysis as the first step to select the best functional monomer and crosslinker and then validated these results. After synthesising MMIP-APTES and MMIP-OA, we assessed their physical characteristics, their ability to remove CLF from spiked human plasma samples and their ability to discriminate between CLF and other TB drugs.

2. Materials and methods

2.1. Materials

CLF was obtained from Sigma-Aldrich, Novartis UK (CAS number 2030-63-9). High-performance liquid chromatography (HPLC)-grade acetonitrile was obtained from Fisher (Pittsburgh, PA, USA). Methyl methacrylate (MMA), a functional monomer; trimethylolpropane trimethacrylate (TRIM), a crosslinker, azobisisbutyronitrile (AIBN), an initiator; 3-aminopropyltrimethoxysilane (APTES); oleic acid (OA); trifluoroacetic acid (TFA); methanol; acetonitrile; isopropanol; hexane; ammonium acetate and chloroform were obtained from Merck, Germany. Blood samples were obtained from the Indonesian Red Cross, Unless otherwise stated, all chemicals were of analytical grade.

The Hyperchem 8.0.10 application is used for molecular geometry optimization to predict the binding sites and calculate the bond energy (ΔE). The sorbent's surface area was analyzed using Brunauer, Emmett, and Teller (BET) Surface Area Quantachrome (Nova 4200E, Boynton Beach, USA).

Morphological evaluation included the use of scanning electron microscopy with energy dispersive spectroscopy (SEM/EDS; JEOL JSM-6360 LA Japan), Fourier-transform infrared (FTIR) spectroscopy (IR Prestige-21, Shimadzu Japan) and particle size analysis (PSA) (Beckman Coulter, LS 13,320, United States). An ultraviolet–visible (UV–Vis) spectrophotometer (Shimadzu, Japan) was used to measure UV absorbance to determine the association constants (K_a) and to generate a Job plot. A digital balance (Ohaus Pioneer, USA), ultrasonicator 50 W 40 kHz (NEY 19H, Houston, Texas, United States), and Centrifuge (Hettich, Germany).

The HPLC conditions for CLF have been described previously [29]. HPLC conditions for CLF have been described previously [29]. This procedure used a Waters Alliance e2695 HPLC device with a Photo Diode Array (PDA) detector, US. As a mobile phase, a gradient elution of orthophosphate buffer and acetonitrile (45:55 v/v, pH 3) and a Reliant C18 column (4.6 × 250 mm, 5 μm) were used. The injection volume is 20 μl with a flow rate of 1.0 ml/min, and the wavelength for CLF detection is 280 nm.

2.2. Computational selection of functional monomer

Computational determination of functional monomers was done by drawing the three-dimensional (3D) structure of the molecule template and monomer using the Hyperchem 8.0.10 application. Structure optimization used the semi-empirical restricted Hartree-Fock (RHF) [30]. The PM3 method is used to optimize complexes between functional monomers and templates using self-consistent fields (SCF) used RHF. Optimization of molecular geometry using the "Polak Ribier" gradient conjugation process, the convergence value is 0.01 kcal [31]. The calculation of ΔE during complex formation is calculated using the equation:

$$\Delta E = (E\ complex) - (E\ CLF\text{-}E\ functional\ monomer)$$

2.3. Computational selection of the crosslinker

Computational determination of functional monomers was done by drawing the three-dimensional (3D) structure of the molecule template and crosslinker using the Hyperchem 8.0.10 application. Structure optimization used the semi-empirical restricted Hartree–Fock (RHF) method [30]. The PM3 method is used to optimize complexes between functional monomers and templates using self-consistent fields (SCF) used RHF. Optimization of molecular geometry using the "Polak Ribier" gradient conjugation process, the convergence value is 0.01 kcal [31]. The calculation of ΔE during complex formation is calculated using the equation:

$$\Delta E = (E_{\ complex}) - (E_{\ CLF}\text{-}E_{\ crosslinker})$$

2.4. Determination of the K_a for the template–functional monomer complex

The computational results of the interaction between monomers and templates were evaluated before polymer synthesis. The evaluation was carried out using UV–Vis spectrophotometry. For this effort, functional monomers were added in increasing amounts up to 0.020 mol/l CLF in isopropanol or chloroform until an excess of functional monomers was reached. The absorbance results obtained and the delta absorbance curve for monomer concentration were used to determine Ka.

2.5. Stoichiometric analysis (Job's plot)

Stoichiometric analysis was performed by systematically varying the molar ratio of CLF-to-MMA in isopropanol to obtain a molar ratio plot. The values used for CLF were 0.002 and MMA 0.01. The total volume of CLF-MMA was 3 ml. The wavelength used was 284 nm, and the absorbance was plotted against the molar concentration of CLF.

2.6. MMIP and magnetic non-imprinted polymer (MNIP) preparation

2.6.1. Fe_3O_4 preparation

To prepare Fe_3O_4, 0.01 mol $(NH_4)_2Fe(SO_4)_2{\cdot}6H_2O$ and 0.02 mol $FeCl_3{\cdot}6H_2O$ were dissolved separately in 100 ml of distilled water. Meanwhile, 50 ml of 3 M NaOH was prepared and placed in a 50 ml syringe, which was used to pierce the rubber of a three-neck flask. Next, 3.92 g of $(NH_4)_2Fe(SO_4)_2{\cdot}6H_2O$ and 5.42 g of $FeCl_3{\cdot}6H_2O$ were weighed and added to this flask. One hundred millilitres of distilled water was added to the three-neck flask filled with nitrogen gas and stirred at 600–1000 rpm at 60 °C (in an oil bath) for 1 h. NaOH was added drop by drop until a black precipitate formed. After 1 h, the precipitated Fe_3O_4 was isolated from the solvent and washed several times with water [32,33].

2.6.2. MMIP-APTES preparation

2.6.2.1. APTES-modified Fe_3O_4. Synthesis began by adding 200 mg of Fe_3O_4 to a vial containing 1 ml of APTES. The mixture was dispersed in methanol and sonicated for 5 min. Then, 500 μl of TFA was added slowly to the solution (heated at 60 °C) for 20 min. The synthesised Fe_3O_4-APTES was rinsed with distilled water and dried at 60 °C for 5 h to obtain Fe_3O_4-APTES [34].

2.6.2.2. Synthesis of MMIP-APTES. Synthesis was carried out in a 20 ml vial containing 1 g Fe_3O_4-APTES dispersed in 5 ml of isopropanol; 0.02 mmol (9.468 mg) CLF and 0.08 mmol (8.5 μl) MMA were added to the mixture and sonicated for 2 h. Then, 20 mmol (128 μl) TRIM and 2 ml AIBN were added to the mixture. The mixture was subjected to a nitrogen flow for 5 min directly into the vial. The vial was closed tightly and sonicated for 15 min. Polymerisation was carried out by heating the mixture in an oven at 60 °C for 20 h. The solid polymer that resulted from the process was still wet, so it was separated and further dried, crushed in a mortar to make a fine powder, and sieved with 80 mesh. The yield is 2.1 % for MMIP-APTES and 3.9 % for MNIP-APTES. The template molecules were extracted by sonicating for 9 h until there were no template molecules (determined by monitoring with a UV–Vis spectrophotometer). MNIP as a control was synthesised in the same way, but the template molecule was omitted [34].

2.6.3. MMIP-OA preparation

2.6.3.1. Fe_3O_4 modification of OA. The synthesis began by coating Fe_3O_4 with OA: 1 ml of OA was added to 500 mg of Fe_3O_4, and the mixture was sonicated for 15 min [35]. Thus producing Fe_3O_4-OA.

2.6.3.2. Synthesis of MMIP-OA. Synthesis was carried out in a vial containing Fe_3O_4-OA. The following was added: 0.02 mmol (9.468 mg) CLF, 5 ml of isopropanol, 0.08 mmol (8.5 μl) MMA, 20 mmol (128 μl) TRIM and 2 ml of AIBN. Nitrogen flowed through the solution for 5 min and the mixture was sonicated for 15 min. The mixture was incubated in an oven at 60 °C for 24 h. The polymer was still wet, so it was separated and dried, ground in a mortar to make a fine powder and sieved with 80 mesh. The template molecules were extracted by sonicating for 9 h until there were no template molecules (determined by monitoring with a UV–Vis spectrophotometer). MNIP was synthesised in the same way, but the template molecule was omitted [34].

2.7. Physical characterization

MMIP and MNIP were characterized by FTIR spectroscopy to evaluate the functional groups in the polymer. MMIP and MNIP, as much as 2 mg, were added with potassium bromide (KBr) for as much as 200 mg, then ground until smooth and made into pellets. The infrared spectrum of MMIP or MNIP was measured at 4000–400 cm^{-1}. The functional groups of MMIP/MNIP sorbents were determined before and after extraction. The polymer surface morphology and elemental composition were observed using SEM-EDS. MMIP or MNIP were placed in silicon and then inserted into the SEM. PSA was used to generate particle size distribution data of MMIP and MNIP. The specific surface area of MMIP and MNIP was determined using BET. In the BET method, the specific surface area flows with nitrogen gas, resulting in the amount of nitrogen gas adsorbed on the surface. For this procedure, 0.5 g of beads was placed in a sample holder and degassed in a nitrogen gas stream at 150 °C for 1 h. Nitrogen gas adsorption was carried out at 210 °C, while the desorption was carried out at room temperature. The instrumental values obtained in the desorption step were used to calculate the specific surface area of the beads.

2.8. Evaluation of the adsorption capacity

CLF solution at 0, 0.25, 0.5, 0.75, 1, 1.5, 2 and 2.5 mg/l was used to evaluate the adsorption capacity of the MMIP-APTES and MMIP-OA sorbents. For this experiment, 1.5 ml of CLF solution was added to a vial containing 20 mg of MMIP sorbent, then allowed to

stand for 24 h at room temperature. Next, the area under curve was measured using HPLC. The experiment was also performed using MNIP sorbent. Langmuir and Freundlich isotherm adsorption curves were used to analyze MMIP adsorption capacity results.

2.9. Use of MMIP to extract CLF from human plasma

2.9.1. Optimization of the extraction conditions

For optimization, 20 mg of MMIP-APTES or MMIP-OA was weight in a 5 ml vial. Then a conditioning step was carried out by adding 1 ml of chloroform and sonicating for 10 min, separating MMIP-APTES or MMIP-OA with an external magnet and discarding the supernatant. The loading stage involved adding 1 ml of 2 mg/l CLF standard solution in chloroform then sonicating MMIP-APTES or MMIP-OA for different times (10, 15, 20, 25, 30 and 60 min), separating MMIP-APTES or MMIP-OA with an external magnetic and discarding the supernatant. MMIP-APTES or MMIP-OA was washed with 1 ml of water, sonicated for 5 min and then separated with an external magnet. The supernatant was separated and filtered, and then injected into the HPLC instrument. Finally, the elution stage involved adding 1 ml of isopropanol, sonicating it for 10 min and then separating MMIP-APTES or MMIP-OA with an external magnet. The supernatant was injected into the HPLC instrument [17].

2.9.2. Validation of the optimized extraction procedure to extract CLF from spiked human plasma samples

First, samples were prepared by adding 25 mM ammonium acetate (pH 9) to plasma to reduce proteins; this step increases recovery. The samples were centrifuged at 6000 rpm for 60 min. Centrifugation was done to separate plasma and proteins after adding ammonium acetate and to produce clear plasma. After centrifugation, the clear part of the plasma is taken. Finally, 2 mg/l CLF was added to the treated plasma [36], the concentration was used to see the capability of the material that has been synthesised on selectively bind to CLF in blood matrices. Next, 20 mg of MMIP-APTES or MMIP-OA was weighed in a 5 ml vial. A conditioning step was carried out by adding 1 ml of chloroform, sonicating it for 10 min, separating MMIP-APTES or MMIP-OA with an external magnet and discarding the supernatant. In the loading stage, MMIP-APTES or MMIP-OA was added to CLF-spiked blood plasma, sonicated for the optimal time (determined according to section 2.9.1) and separated with an external magnet; the supernatant was discarded. MMIP-APTES or MMIP-OA was washed with 1 ml of water, sonicated for 5 min and then separated with an external magnet; the supernatant was separated. Finally, for elution, 1 ml of isopropanol was added; the mixture was sonicated for 10 min and then separated with an external magnet. The solution from the elution stage was injected into the HPLC instrument [17].

2.9.3. Determination of MMIP-SPE selectivity for CLF compared with other TB drugs in spiked human plasma

First, samples were prepared by adding 25 mM ammonium acetate (pH 9) to plasma to reduce proteins; this step increases recovery. The samples were centrifuged at 6000 rpm for 60 min. Treated blood plasma was spiked with CLF, isoniazid (INH), rifampicin (RIF) and ethambutol (ETH), each at 2 mg/l. The spiked plasma was then passed through MMIP-SPE or MNIP-SPE sorbents. Analysis of the elution results was performed using HPLC. The percentage recovery was calculated for each compound on each MMIP and MNIP sorbent [37].

3. Results and discussion

3.1. Computational selection of a functional monomer

Functional monomers influence the success of MMIP manufacturing. In MMIP pre-polymerisation, the functional monomer interacts with the template molecule [14]The monomer provides functional groups that can form complexes with the template molecule via covalent or non-covalent interactions. The accuracy and selectivity of MMIP and MIP recognition depend on the strong interaction between the template molecule and the monomer, which affects the affinity of MMIP and MIP.

We analyzed the interaction between CLF and each functional monomer by calculating ΔE and evaluating the non-covalent bonds formed in the complex, especially hydrogen bonds. First, we checked whether the interaction occurred at the correct position by examining the electronic data of the CLF, which is seen in the total charge density on the contour map and the electrostatic data—prediction of interactions that occur between functional monomers and templates using electrostatic potential [31].

The formation of stable complexes in the synthesis of MMIP and MIP occurs when producing low ΔE computationally on the complex that occurs between the interaction of functional monomers and CLF [31,38]. Optimization of the functional monomer complex and template using the PM3 method to find the best functional monomer for CLF. This method is used with SCF at the RHF level. The selection of the PM3 method was based on the consideration that this method is fast, accurate results in the simulation of intramolecular and intermolecular interactions, and can use large molecules. We calculated ΔE during complex formation. Table 1 shows ΔE for the interaction between the template (CLF) and 11 functional monomers commonly used to produce printed polymers. ΔE

Table 1
Template-functional monomer complex ΔE values.

Template-functional monomer complex	ΔE (Kcal/mol)	Compotition
Clofazimine-Itaconic Acid	−24,83	1:4
Clofazimine-Acrylamide	−21,46	1:4
Clofazimine-Methyl methacrylate	−29,96	1:4

indicates the formation of complex stability. The lower and most negative ΔE value, A low ΔE value will produce stable complex interactions, resulting in selective MMIP and MIP synthesis results. The lowest energy interaction energy of the three complexes between the CLF structure and functional monomers methyl methacrylate (MMA), itaconic acid (ITA) and acrylamide (AAM), with ΔE of −29.96, −24.83 and −21.46 kcal mol/l, respectively. Each complex with low ΔE indicates that the formed MMIP and MIP will provide very good selectivity. Initial predictions using computation in determining the amount of monomer that interacts with the template produce reaction stoichiometry for determining the MMA: CLF molar ratio that will be used in the synthesis process. Description of complex interactions between CLF and monomers, namely in MMA monomers (Fig. 1a), ITA (Fig. 1b) and AAM (Fig. 1c). In computational testing, the interaction between template-monomer did not occur due to the formation of hydrogen bonds in the template-monomer complex. Instead, the interaction is mediated by dispersion forces (also known as the van der Waals forces) [39]. This force arises because local fluctuations in one particle induce, through the propagation of electromagnetic waves, a response that appears due to correlation in the other particle. The dispersion force is based on the number of dipole interactions. The attractive potential due to dispersion forces between two particles depends on the distance [40]. Computational simulations found that four MMAs would form a stable complex with one CLF showing the lowest ΔE (Table 1). We further validated the computational results by determining the stoichiometry with Job's plot.

3.2. Computational selection of a crosslinker

A crosslinker fixes the functional monomer groups around the template molecule, allowing the formation of a crosslinked rigid polymer. After the removal of the template molecule, the hole formed must completely complement the target molecule in form and functional group. The type and amount of crosslinker have a major influence on the selectivity and binding capacity of a MIP. When the crosslinker concentration is too low, the MIP cannot maintain a stable cavity configuration due to the low degree of cross-linking. However, when the crosslinker concentration is too high, there will be fewer recognition sites per unit mass of MIP. The most frequently used crosslinkers are TRIM, divinylbenzene (DVB), and ethylene glycol dimethacrylate (EGDMA) [41]. We used Hyperchem software to evaluate these three crosslinkers; the process involves bringing the crosslinker close to the template. Crosslinkers with low ΔE will compete with functional monomers to form complex bonds with the template, and will affect the synthesis process of MMIPs and MIPs, which will ultimately affect their analytical performance. We chose the crosslinker with the highest ΔE because it would have a weaker interaction with the template [30,41]. Polymer selectivity will increase when the crosslinker-template complex interaction is weaker than the functional monomer-template interaction [30]. Based on the results in Table 2, we performed computational modeling for the cosslinkers EGDMA, TRIM, and DVB. TRIM has a higher ΔE (−3.46 kcal mol/l) compared to DVB (−5.93 kcal mol/l) and EDGMA (−7.13 kcal mol/l). Thus, TRIM was selected as the best crosslinker for CLF imprinting in the synthesis of MMIPs and MIPs. Fig. 2 illustrates the interaction between CLF and each crosslinker, namely in the crosslinker DVB (Fig. 2a), TRIM (Fig. 2b) and EDGMA (Fig. 2c).

3.3. Determination of the K_a for the template–functional monomer complex

We used UV–Vis spectrophotometry to determine the K_a for template–functional monomer complexes. We considered MMA, ITA and AAM, based on the computational results. The K_a is associated with the binding affinity of the functional monomer to the template. When calculating the CLF–MMA K_a, we added an increasing amount of functional monomer to the CLF solution (0.05 mol/l) in four solvents, namely isopropanol, acetonitrile, chloroform and a mixture of acetonitrile and isopropanol (1:2). We recorded and plotted delta absorbance. Ka calculations are carried out by collecting absorption data and making graphs based on the intersection using "Benesi Hildebrand" data analysis. The highest Ka value for the CLF–MMA complex is in isopropanol solvent (Table 3). CLF (pKa = 8.51) will bind more strongly to MMA because this functional monomer is a strong base (pKa = 6.8) in isopropanol (pKa = 17.1) compared with ITA (pKa = 3.84) [42] and AAM (pKa = 15.35). The selected porogen isopropanol, which is a polar protic solvent, will prevent hydrogen bonding between the template and the functional monomer in the pre-polymerisation solution [43]. The higher K_a for MMA compared with ITA and AAM means that the bond strength for the CLF–MMA interaction is greater than that of the CLF–ITA and CLF–AAM interactions [14].

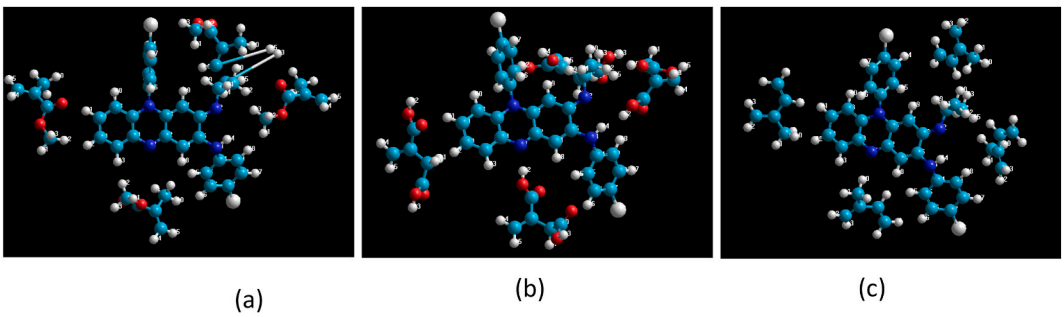

Fig. 1. Illustrations of interactions between Clofazimine and functional monomers: (a) MMA, (b) ITA, and (c) AAM.

Table 2
Template-crosslinker complex ΔE values.

Template-crosslinker complex	ΔE (Kcal/mol)	compotition
Clofazimine-TRIM	−3.46	1:1
Clofazimine-DVB	−5.93	1:1
Clofazimine-EDGMA	−7.13	1:1

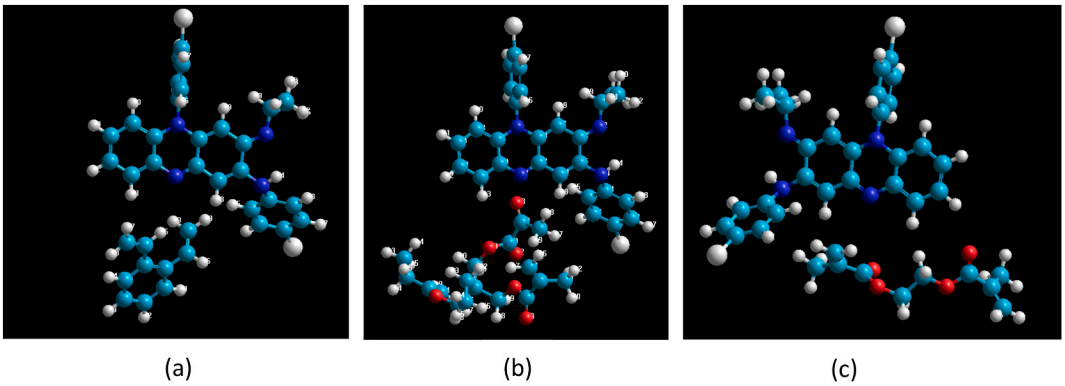

Fig. 2. Illustrations of interactions between Clofazimine and crosslinker: (a) DVB, (b) TRIM and (c) EDGMA.

Table 3
Association constant value of CLF.

Monomer	Solvent	K_a (M^{-1})
MMA	Isopropanol	813.85
	Chloroform	174.94
	Acetonitrile	99.24
	Acetonitrile: Isopropanol	182.73
ITA	Isopropanol	297.36
	Chloroform	99.13
	Acetonitrile	283.55
	Acetonitrile: Isopropanol	148.79
AAM	Isopropanol	214.77
	Chloroform	23.10
	Acetonitrile	244.69
	Acetonitrile: Isopropanol	155.93

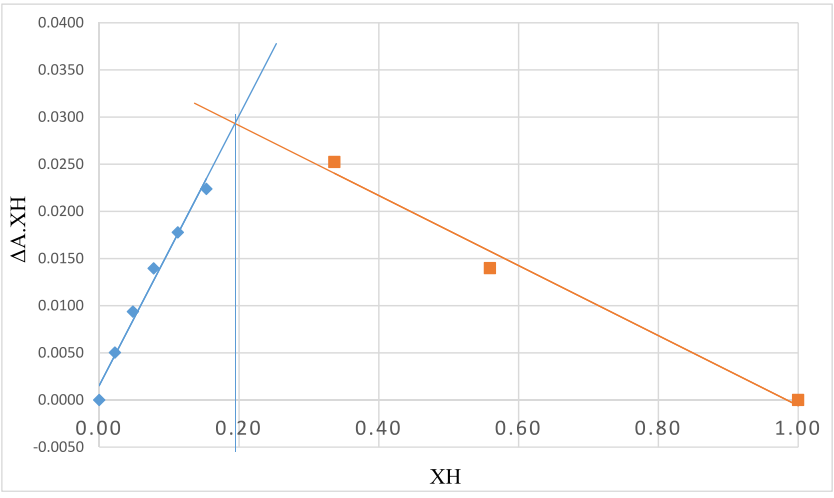

Fig. 3. Jobs plot of CLF-MMA complex.

3.4. Stoichiometry analysis (Job plot)

Analysis of complex molecular ratios may assist in the design of a polymer synthesis protocol. We evaluated the pre-polymerisation CLF–MMA complex by using the Job's Plot method (Fig. 3). A method is often used to determine the stoichiometry of complex interactions, and this analysis is applied in various techniques, such as UV–Vis spectrophotometry [44]. This method is based on

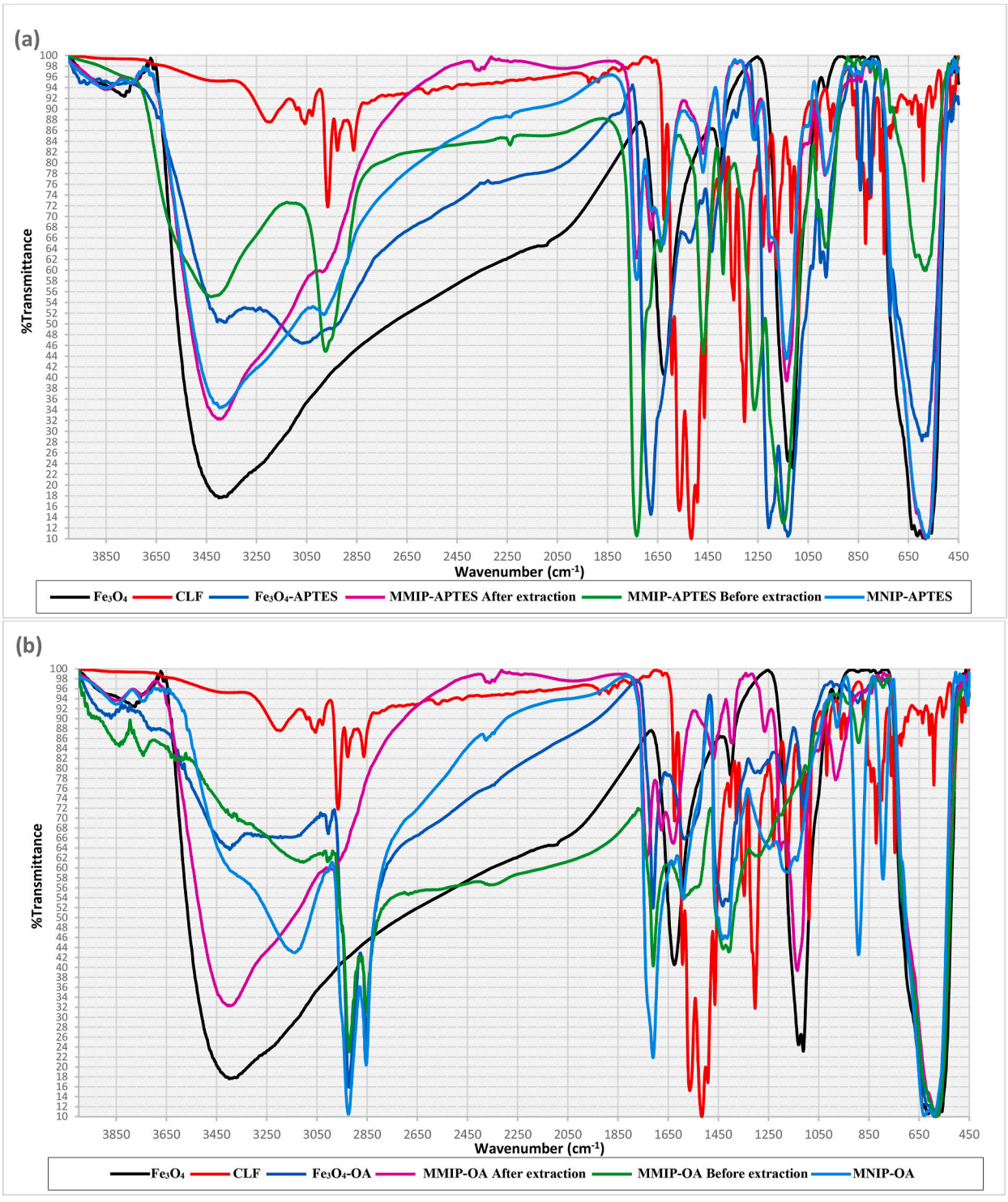

Fig. 4. Spectrum of spectrophotometry Infra red: (a) MMIP-APTES and (b) MMIP-OA

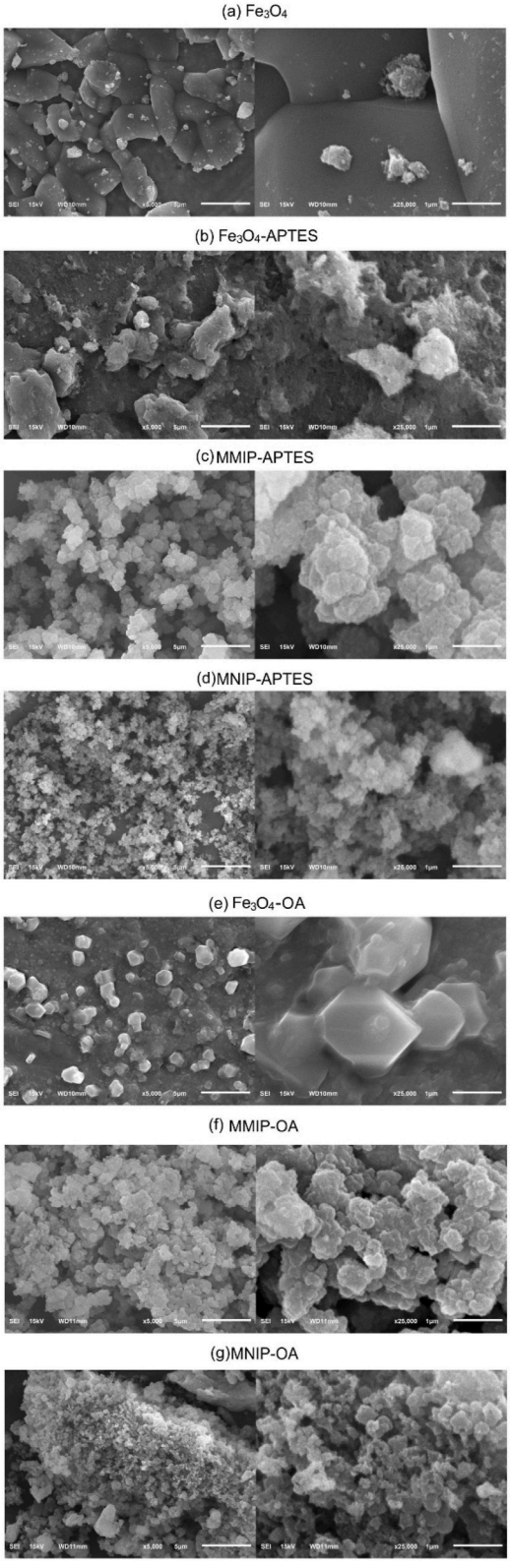

Fig. 5. Scanning electron microscope (SEM) of (a) Fe_3O_4, (b) Fe_3O_4-APTES, (c) MMIP-APTES, (d) MNIP-APTES, (e) Fe_3O_4-OA,(f) MMIP-OA and (g) MNIP-OA.

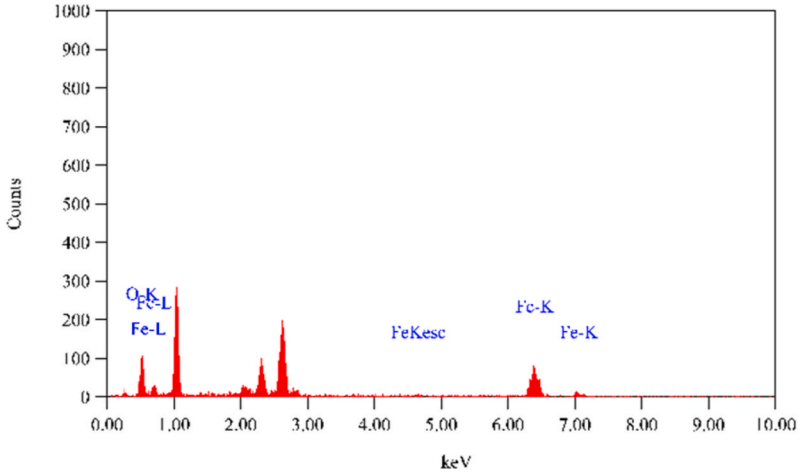

(a)

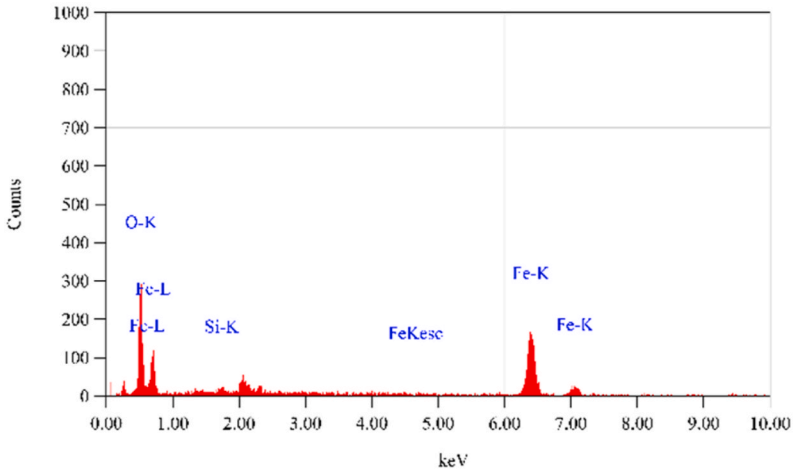

(b)

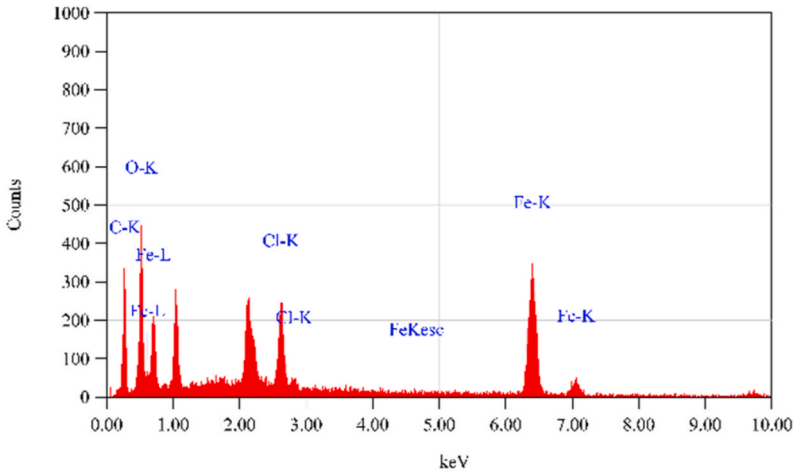

(c)

Fig. 6. EDS analysis of (a) Fe_3O_4, (b) Fe_3O_4-APTES and (c) Fe_3O_4-OA.

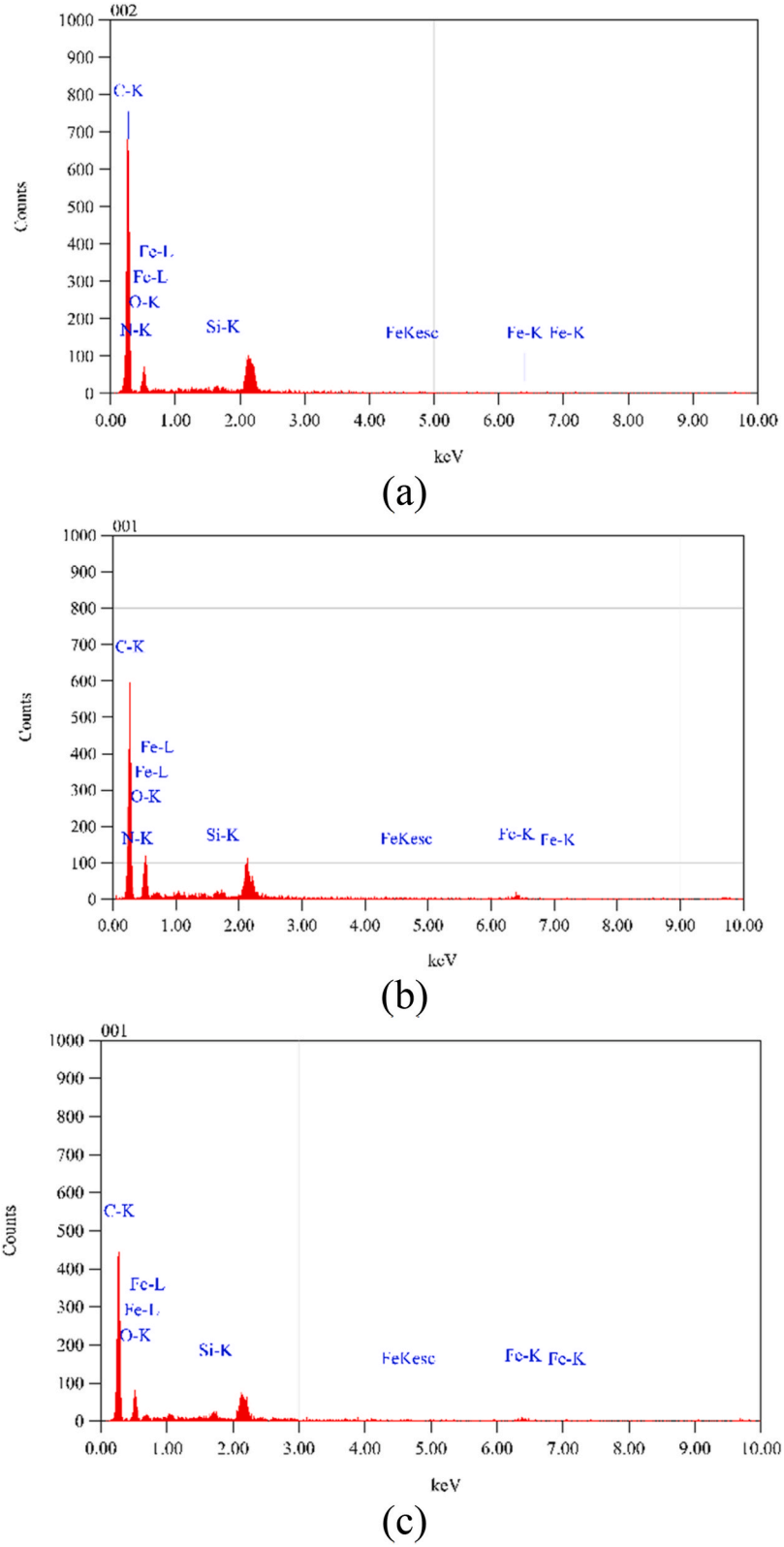

Fig. 7. EDS analysis of (a) MMIP-APTES Before extraction, (b) MMIP-APTES after extraction and (c) MNIP-APTES (d) MMIP-OA Before extraction, (e) MMIP-OA after extraction and (f) MNIP-OA

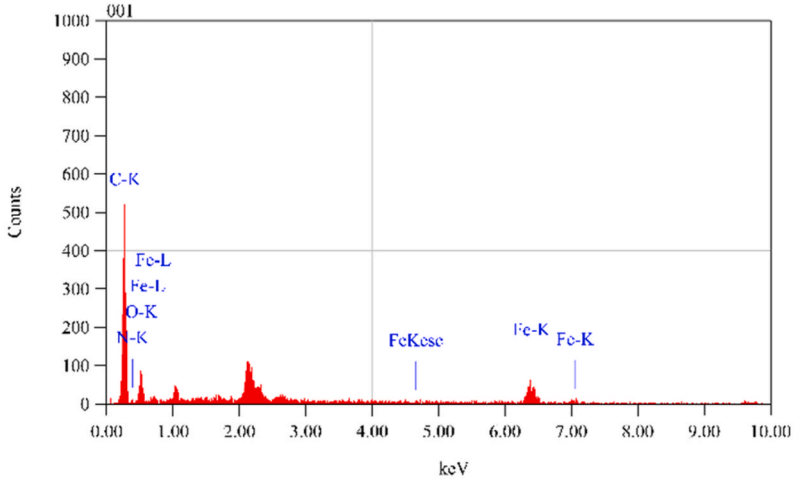

(d)

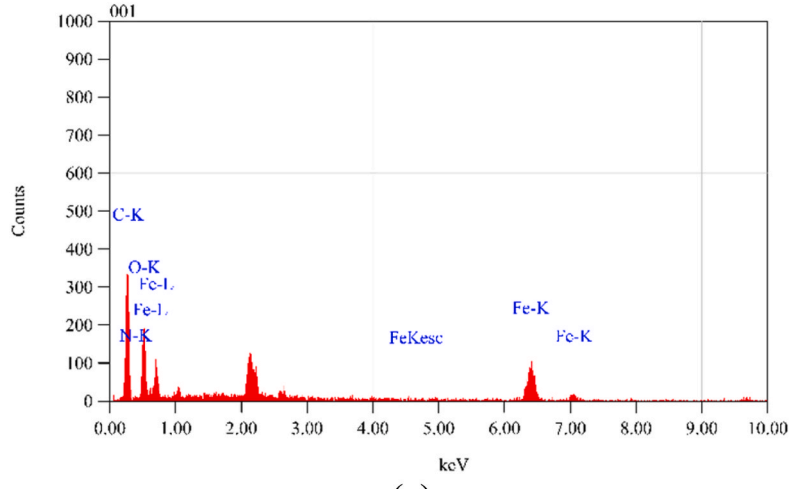

(e)

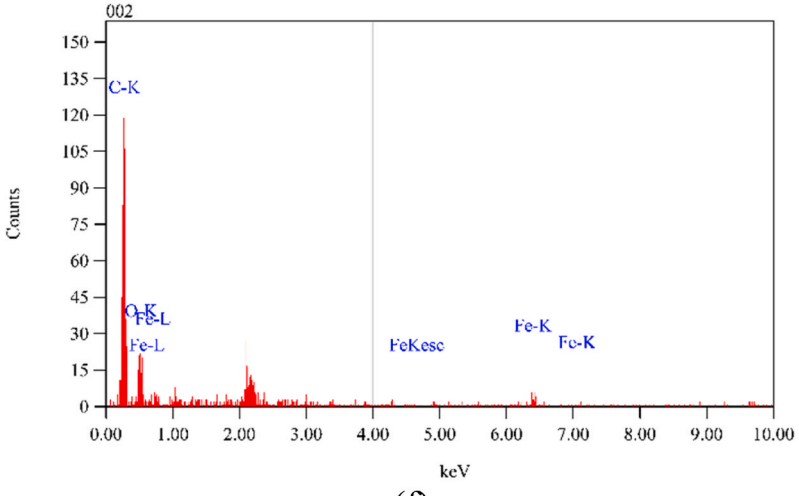

(f)

Fig. 7. (*continued*).

observed spectral changes for both the guest molecule (functional monomer) and the host molecule (CLF). Measurement of the absorbance of both component solutions in isopropanol solvent at a wavelength of 284 nm. We found that the absorbance increased as the CLF concentration increased, reaching a maximum at a template-to-functional monomer molar ratio of 1:4. The absorbance decreases when more functional monomers are added. This is because higher molar concentrations of some monomers will cause such effects [44]. This shows that one molecule of CLF and four molecules of MMA (molar ratio 1:4) produce the most stable pre-polymerisation complex, which confirms the computational results.

3.5. Physical characterization

3.5.1. FTIR spectroscopy

The characteristic peaks of MMIP and MNIP indicate the vibration types of functional groups in IR spectrum at 1735 and 1677 cm^{-1}, respectively, originate from the stretching vibration of the double bonds in the –C═O and –CH═CH_2 groups of the TRIM molecule. These peaks indicate the existence of a TRIM structure and thus successful synthesis [45,46].

Fig. 4a shows the FTIR spectrum of MMIP-APTES. There are CLF peaks (red band) for N–H groups at 1563−1620 cm^{-1} and C═N groups at 1625.09 cm^{-1} [46]. There is a broad peak in the black band (Fe_3O_4) showing functional groups Fe–O at 589 cm^{-1} [47]. Fe_3O_4-APTES (blue band) shows a broad peak at 596.16 cm^{-1} indicating Fe–O, and at 1000.35 cm^{-1}, which is from Si–*O*–Si groups (based on the literature, the Si–*O*–Si band is reported to be at 1015–1073 cm^{-1}). Before extraction, MMIP-APTES had an Fe–O band at 589.42 cm^{-1} and a CLF band at 1629.88 cm^{-1}. After extraction, there is an Fe–O band at 587.47 cm^{-1} but no CLF band. MNIP-APTES shows a Fe–O band at 583.76 cm^{-1} as well as a band in the range of 1015–1073 cm^{-1}, indicative of Si–*O*–Si [48].

Fig. 4b shows the FTIR spectrum of MMIP-OA. There are CLF peaks (red band) for N–H at 1563−1620 cm^{-1} and C═N at 1625.09 cm^{-1} [49]. There is a broad peak in the black band (Fe_3O_4) showing Fe–O at 582.60 cm^{-1}. Fe_3O_4-OA (blue band) shows a broad peak at 589.98 cm^{-1}, indicating Fe–O [47], and at 2852.15 and 2922.25 cm^{-1}, indicating –CH_2– and –CH_3 stretching, respectively, of OA. The bands at 1432.30 cm^{-1} and 1586.20 cm^{-1} are attributed to the stretching vibrations of the –COO functional group, indicating that the Fe_3O_4 surface was successfully coated with OA. Before MMIP-OA extraction, there is an Fe–O band at 589.98 cm^{-1} and a CLF band (for N–H) at 1550–1620 cm^{-1}. After MMIP-OA extraction, there is an FeO band (589.98 cm^{-1}) but no CLF band. MNIP-OA shows an Fe–O band at 589.98 cm^{-1} and a band for –CH2– and –CH_3 stretching of OA at 2852.15–2922.25 cm^{-1}. The bands at 1710.01 cm^{-1} (CO group) and 1404.35 and 1586.20 cm^{-1} (–COO functional group) indicate that OA successfully coated the MNIP surface [50].

3.5.2. SEM/EDS

3.5.2.1. SEM. MMIP particles were visualized using SEM at 5000 × and 25,000 × magnification. The Fe_3O_4 magnetic nanoparticles, shown in Fig. 5a, have an irregular crystalline shape. The morphology of Fe_3O_4-APTES particles in Fig. 5b shows an irregular crystal shape, Fe_3O_4-OA in Fig. 5e shows a regular crystal shape, and surface morphology analysis shows a hexagonal particle agglomeration shape. In SEM analysis, it can be seen that the surfaces of Fe_3O_4-OA and Fe_3O_4-APTES are smoother than Fe_3O_4 nanoparticles because the Fe_3O_4 magnetic nanoparticle layer is coated with SiO and OA, respectively. MMIP-APTES and MNIP-APTES (Fig. 5c and d) and MMIP-OA and MNIP-OA (Fig. 5f and g) show a round and uniform particle shape and have a flat surface with many holes [51]The most significant difference between MMIP and MNIP is that MMIP's distribution is more homogeneous compared to MNIP. This phenomenon may be related to the presence of template molecules in the polymerisation medium. MMIP's structural properties indicate higher adsorption ability.

3.5.2.2. EDS. Based on Fig. 6a, the percentage of Fe and O in Fe_3O_4 nanoparticles is 57.25 % and 42.75 %, respectively. The chemical composition of Fe_3O_4-APTES (Fig. 6b) is 0.98 % Si and 41.17 % Fe. The weak Si and strong Fe peaks indicate the formation of a thin silica shell on the surface of the Fe_3O_4 nanoparticles. Finally, Fig. 6c shows the chemical composition of Fe in Fe_3O_4-OA. The EDS results of MMIP-OA before extraction contained the chemical composition C, O, Fe, and N, in MMIP before extraction (67.34 %, 15.12 %, 3.56 %, and 13.98 %) and MMIP after extraction (59, 52 %, 24.36 %, 6.80 % and 9.33 %) and the chemical composition of C, O, Fe in MNIP (98.77 % and Fe elements 1.23 %). There were OA elements, namely C and O [50].

EDS analysis provides the chemical composition of the nanoparticles and the percentage of the elements [52]. Before extraction, the chemical composition MMIP is 65.28 % C, 12.60 % O, 0.01 % Si, 0.06 % Fe and 22.05 % N (Fig. 7a). After extraction, the chemical composition of MMIP is 63.71 % C, 20.61 % O, 0.15 % Si, 0.71 % Fe and 14.82 % N (Fig. 7b). Finally, the composition of MNIP-APTES

Table 4
The result of Particle size analysis (PSA).

No	Polymer	Particle Size (μm)
1.	Fe_3O_4	0.15
2.	Fe_3O_4-APTES	0.13
3.	MMIP-APTES	0.14
4.	MNIP-APTES	0.58
5.	Fe_3O_4-OA	0.11
6.	MMIP-OA	0.29
7.	MNIP-OA	0.18

is 78.49 % C, 20.42 % O, 0.24 % Si and 0.85 % Fe (Fig. 7c). The presence of a weak Si peak and a strong Fe peak indicates the formation of a thin silica shell on the MMIP-APTES and MNIP-APTES surfaces [51]. MMIP before extraction contains 3.56 % Fe and 13.98 % N (Fig. 7d). After extraction, MMIP contains 6.80 % Fe and 9.33 % N (Fig. 7e). Finally, MNIP contains 1.23 % Fe and 98.77 % other elements (Fig. 7f).

3.5.3. PSA

With PSA, we generated particle size distribution data. MIP particle laser diffraction analysis provides information regarding volume size distribution [53]. In MMIP synthesis, the physical properties of nanoparticles with small and uniform sizes are required, so that a more stable protective layer is formed [54]. Table 4 shows that MMIP-APTES particles were notably smaller than the MMIP-OA particles.

3.5.4. BET

The BET method assumes that there are uniform pore walls. The MIP surface area and porosity are influenced by the presence of template molecules in MIP polymerisation [53]. We detected the BET surface area with nitrogen adsorption measurements. As shown in Table 5, the specific surface area was 2913.07 m^2/g for MMIP-OA and 2874.51 m^2/g for MMIP-APTES. MMIP has a specific surface area that is almost three times larger than MNIP due to the presence of cavities formed by the imprinting process. SEM and BET characterization results show an increase in the surface area of MIP due to the imprinting of template molecules [30]. The large surface area is likely due to the small particle size according to the PSA analysis (Table 4) and this is correlate with the research by Mukami & Batlokwa 2018, and Stevens & Batlokwa, 2017 [55,56], the size is small enough to be associated with an increase in surface area which results in increased sorbent capacity. The smaller the particle size, the higher the surface area.

3.5.5. VSM

The magnetization curve of the product was obtained using a PPMS-9T vibrating sample magnetometer (VSM) (VSM OXFORD1.2H) with an applied field between −15,000 and 15,000 Oe at room temperature.

The saturation magnetization of MMIP-APTES (21.1 emu/g) showed in Fig. 8a and MMIP-OA (49.9 emu/g) showed in Fig. 8b is smaller compared to Fe_3O_4 (50.0 emu/g). Despite the saturation magnetization of MMIPs, MMIPs still show sufficient attraction for separation. The decrease in magnetization value is caused by the presence of APTES and OA coatings and a molecular imprinting layer on the surface of the Fe_3O_4 [57]. MMIP features a typical magnetic hysteresis loop. Nearly zero coercivity and zero remanence in the magnetization curve indicate the are superparamagnetic. This can be ascribed to the small size of MMIP-APTES and MNIP-OA which are critical sizes of superparamagnetism [58]. The output is a hysteresis curve, which shows the relationship between the induced magnetic flux density and the magnetization force and provides important information about magnetic saturation, remanence, and coercivity and the degree of residual magnetism remaining in the material. MMIP-APTES had a lower magnetization value, possibly because the level of residual magnetism in the polymer decreases [59], but it still provides sufficient magnetization effect [57].

Based on Sobiech et al. [60] and Wo'znica et al. [28] Increasing the number of functionalized siloxane cores decreases the percentage of organic layers in the material and results in a thin shell layer on the molecularly imprinted polymer. The thickness of the imprinted layer affects the polymer's magnetic properties but does not affect the adsorption process on the polymer surface. The results show that with the presence of the Si layer on MMIP-APTES, the magnetization decreases compared to oleic acid (without the Si layer).

3.6. Evaluation of the adsorption capacity

We determined the adsorption capacity of MMIP and MNIP by using adsorption isotherm models. The adsorption capacity results are shown in Table 6, the K_F value for MMIP-APTES is 1.48 mg/g and MNIP-OA 35.56 mg/g. Differences in polymer adsorption intensity indicate large differences in binding site affinity [30,61]. Based on the correlation coefficients, the Langmuir isotherm best described MMIP-OA, indicating the homogeneous nature of the binding sites, while the Freundlich isotherm best described MMIP-APTES, indicating the heterogeneous nature of the binding sites. These data indicate that MMIP-APTES has heterogeneous binding sites compared to MMIP-OA. The differences in binding sites indicate differences in the intensity of polymer adsorption ability [62]. The results also show that chloroform is the best solvent in adsorption ability testing.

Table 5
The result of Brunauer, Emmett and Teller (BET).

No	Polymer	Surface Area (m^2/g)
1.	Fe_3O_4	314.66
2.	Fe_3O_4-APTES	343.95
3.	MMIP-APTES	2874.51
4.	MNIP-APTES	1201.29
5.	Fe_3O_4-OA	11.81
6.	MMIP-OA	2913.07
7.	MNIP-OA	974.38

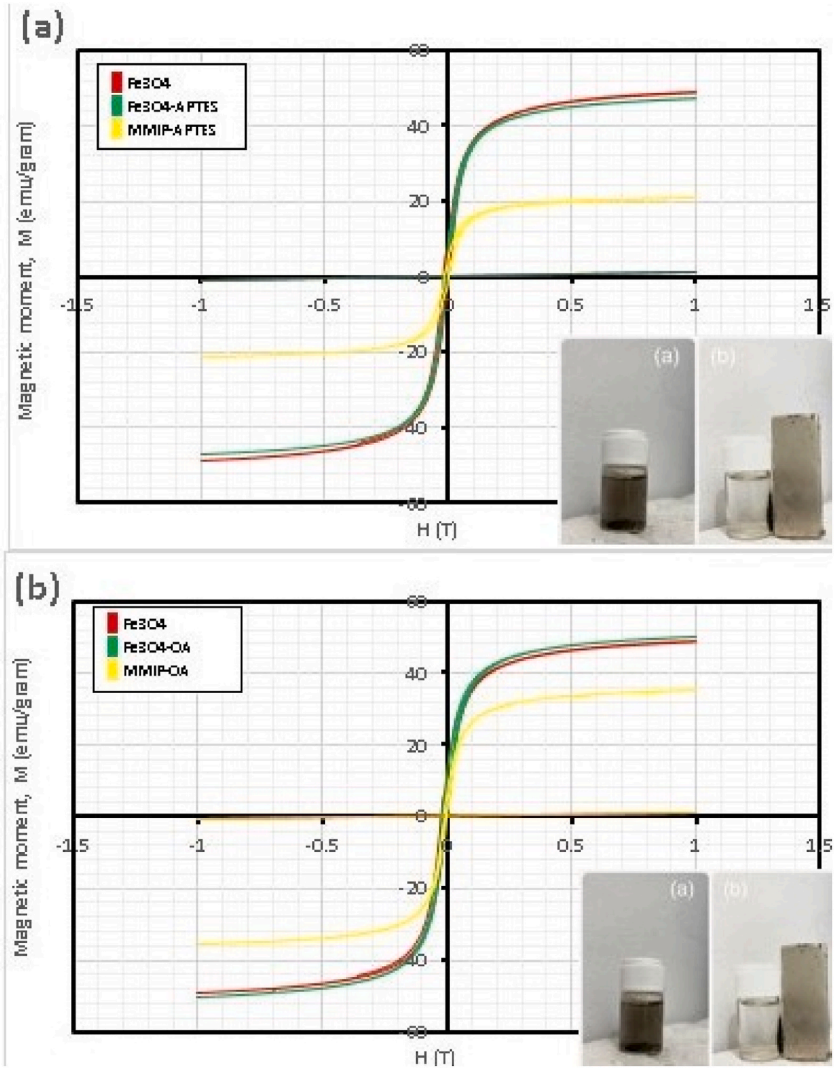

Fig. 8. Vibrating Sample Magnetometer (VSM) curve of: (a) MMIP-APTES and (b) MMIP-OA.

Table 6
The result of adsorption capacity.

	Freundlich isotherm					Langmuir isotherm				
	1/n	n	$\log K_F$	K_F (mg/g)	R^2	1/Qm	Qm	$1/K_L \cdot Qm$	K_L	R^2
MMIP-APTES	−2.522	−0.396	0.171	1.484	0.9944	12.289	0.081	0.465	26.454	0.9528
MNIP-APTES	−2.954	−0.338	−3.292	0.001	1.0000	8.926	0.112	−0.249	19.214	0.9915
MMIP-OA	0.397	2.518	1.551	35.563	0.9942	7.259	0.138	−0.064	−113.460	0.9998
MNIP-OA	−0.278	−3.601	0.857	7.198	0.7958	3.625	0.276	2.423	−56.659	0.9993

3.7. Use of MMIP to extract CLF from human plasma

3.7.1. Optimization of the extraction conditions

We optimized the extraction conditions by using a standard solution of 2 mg/l CLF in chloroform, which was the best solvent in the absorption capacity test. We investigated the following SPE parameters: conditioning, loading, washing, and elution solvent. First, we used chloroform to determine the solvent in the conditioning step and conducted experiments on vials containing MMIP and MNIP. Changes in the surface area and pore volume of the polymer due to organic solvents will affect the polymer network [30]. We used chloroform for the loading solvent. We had to consider the influence of the loading solvent's polarity to ensure good CLF–MMIP interaction. We chose chloroform because it had relatively low polarity and is not expected to interfere with the MMIP–CLF interaction.

Based on optimization of the adsorption conditions, the adsorption percentage of CLF was optimal when we used chloroform as a solvent. We performed the loading step at six sonication times – 10, 15, 20, 25, 30 and 60 min. The next step is to carry out the washing optimization stage. Washing is an essential step in the MMIP-SPE procedure because a standard procedure to reduce nonspecific absorption problems is the appropriate selection of solvents at the washing stage. Strong trace–analyte interactions must be destroyed to achieve high extraction recoveries. Protonation of CLF is expected to encourage disruption of the hydrogen bonds between CLF and MMIPs [30]. We evaluated elution with 1 ml of elution solvent and six loading contact times – 10, 15, 20, 25, 30 and 60 min – to determine the best recovery.

We found that the optimal loading time was 20 min for MMIP-APTES and 60 min for MMIP-OA. The final recovery at a loading time of 20 min was 104.43 % ± 11.75 % for MMIP-APTES and 33.95 % ± 8.19 % for MNIP-APTES (Fig. 9a). The final recovery at a loading time of 60 min was 105.07 % ± 14.71 % for MMIP-OA and 95.42 ± 32.03 % MNIP-OA (Fig. 9b).

3.7.2. Validation of the optimized extraction procedure to extract CLF from spiked human plasma samples

We determined the real performance of MMIP-APTES and MMIP-OA in MMIP-SPE (MMIP-SPE-APTES and MMIP-SPE-OA, respectively) to extract CLF from human plasma using blood plasma spiked with 2 mg/l CLF in chloroform. We compared MMIP-SPE with MNIP-SPE (using MNIP-APTES or MNIP-OA – MNI-SPE-APTES and MNI-SPE-OA, respectively). We performed the test three times to evaluate the repeatability of each test and calculated the recovery and imprinting factor (IF). The IF indicates the distribution of a particular analyte in the MIPs versus the NIPs; an IF > 1 indicates good printing [14]. MMIP-SPE-APTES resulted in an average recovery of 92.3 % ± 6.1 % while MNIP-SPE-APTES provided an average recovery percentage of 56.7 % ± 4.6 % with an IF of 1.6 (Table 7). The chromatograms for MMIP-SPE-APTES and MNIP-SPE-APTES are shown in Fig. 10a. MMIP-SPE-OA had an average recovery of 51.5 % ± 8.1 % while MNIP-SPE-OA had an average recovery of 34.1 % ± 5.0 % with an IF of 1.5 (Table 7). The chromatogram for MMIP-SPE-OA and MNIP-SPE-OA are shown in Fig. 10b (see Fig. 11).

The higher IF of MMIP-SPE-APTES compared with MMIP-SPE-OA indicates better printing in MMIP-APTES, likely because MMIP-APTES particles are smaller than MMIP-OA particles. Hence, there was stronger attraction to CLF. Based on the recovery results, MMIP-SPE-APTES meets the requirements for recovering analytes from biological samples, which is >80 % [61].

3.7.3. Determination of MMIP-SPE selectivity for CLF compared with other TB drugs in spiked human plasma

We tested the selectivity of MMIPs to extract CLF from blood plasma compared with other TB drugs, namely INH, ETH and RIF. We spiked blood plasma with 2 mg/l of each drug (Fig. 10). The percentage recovery of MMIP-SPE-APTES was 94.6 % ± 10.0 % for CLF, 36.3 % ± 4.6 % for INH, 36.1 % ± 1.8 % for ETH and 22.9 % ± 8.2 % for RIF. The percentage recovery of MMIP-SPE-OA was 86.9 % ± 14.9 % for CLF, 61.1 % ± 5.1 for INH, 22.4 % ± 11.9 % for ETH and 33.2 % ± 8.0 % for RIF.

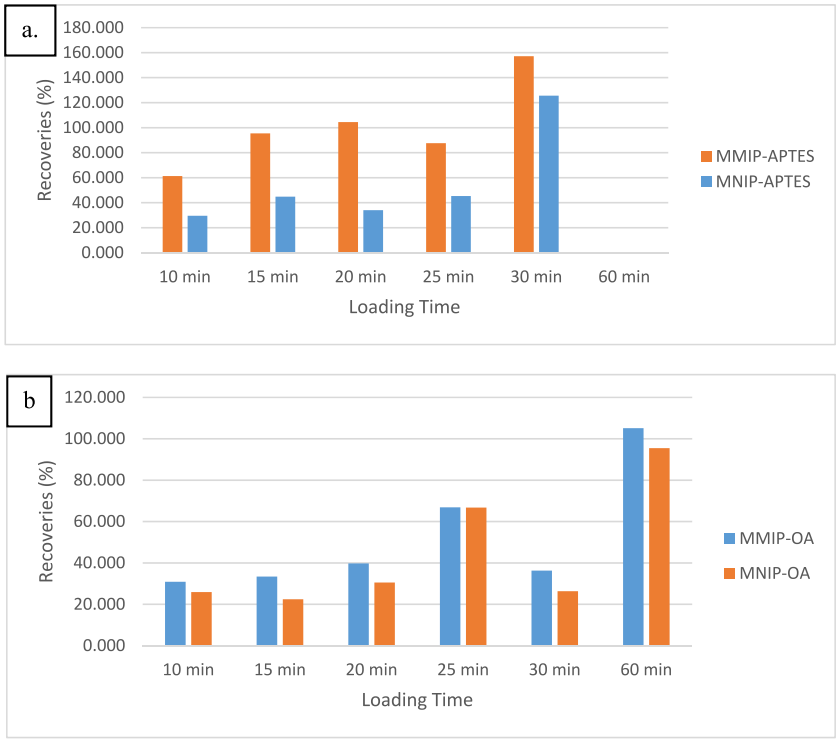

Fig. 9. MMIP-SPE and MNIP-SPE optimization of the extraction conditions graph (a.) MMIP-SPE-APTES and MNIP-SPE APTES (b.) MMIP-SPE-OA and MNIP-SPE-OA.

Table 7
Result of CLF recoveries extracted from human plasma sample.

Polymer	%Recovery	SD	IF
MMIP-SPE-APTES	92.3	6.1	1.6
MNIP-SPE-APTES	56.7	4.6	
MMIP-SPE-OA	51.5	8.1	1.5
MNIP-SPE-OA	34.1	5.0	

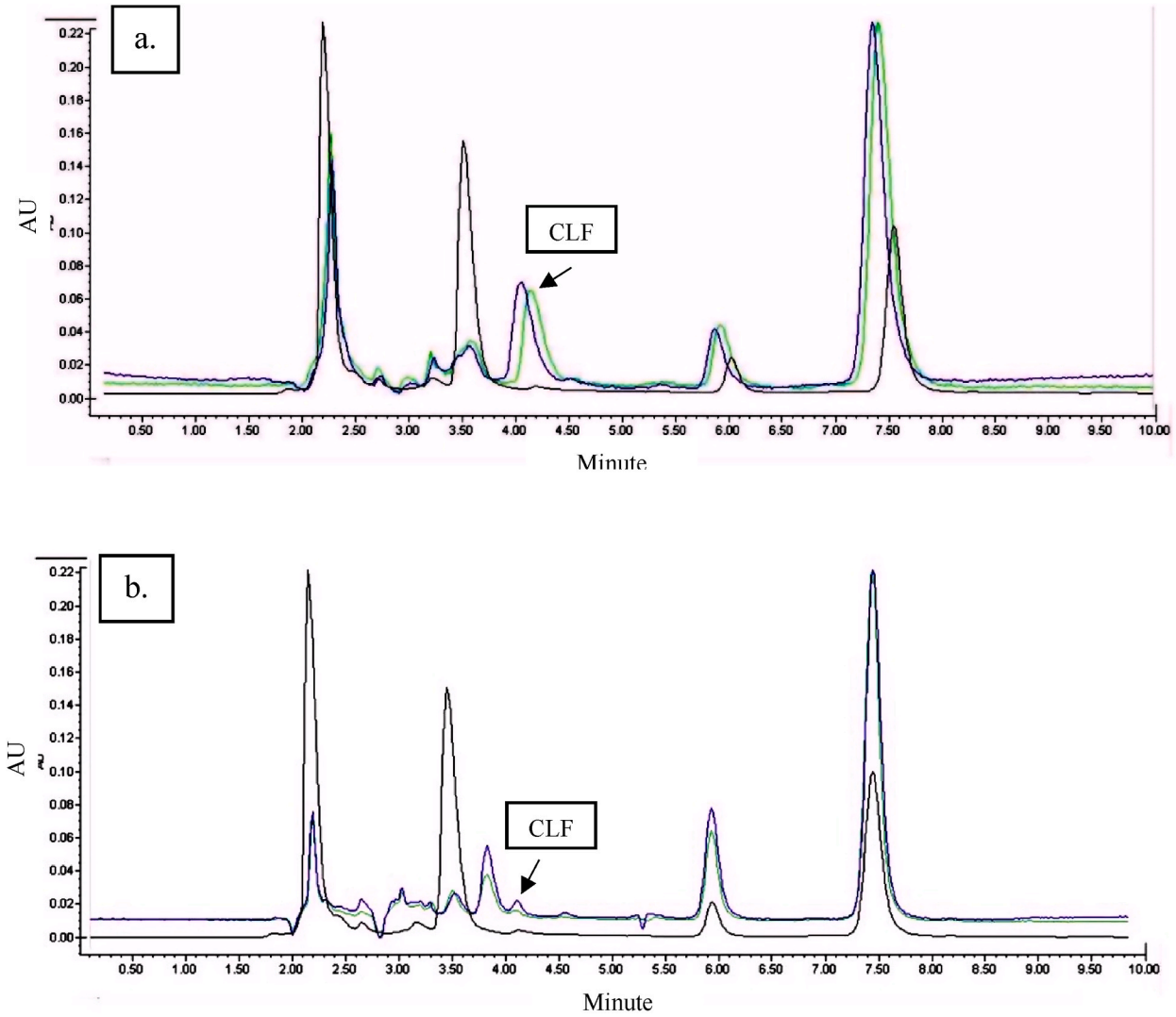

Fig. 10. Chromatogram of MMIP-SPE and MNIP-SPE a) blank serum samples (black), MMIP-SPE-APTES (blue) and MNIP-SPE-APTES (green) b) blank serum samples (black) MMIP-SPE-OA (blue) and MNIP-SPE-OA (green). (For interpretation of the references to colour in this figure legend, the reader is referred to the Web version of this article.)

Overall, MMIP-SPE-APTES showed good selectively from CLF. APTES has been widely used in biosensors and to facilitate the immobilization of biomolecules in polymers. APTES is affinity based because the silane group can bond tightly to silicon or glass substrates, while the amine group can form covalent bonds with carboxyl groups (functional groups commonly found in biomolecules) [63]. Moreover, it showed a faster absorption rate to reach 80 % recovery (20 min) compared with OA (60 min) [31]. OA is a surfactant that is commonly used to stabilise magnetic nanoparticles. Strong chemical bonds are formed between carboxylic acids and amorphous iron and amorphous iron oxide. A layer of OA balances van der Waals forces and the osmotic pressure, and there are two different types of binding energies between OA molecules and the surface of particles [64]. We suspect that the MMIP-APTES bond with CLF is more stable than the MMIP-OA bond with CLF.

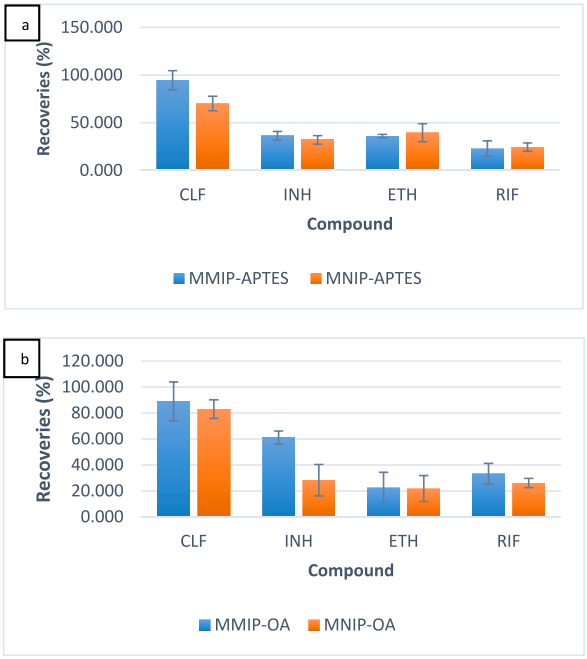

Fig. 11. MMIP-SPE and MNIP-SPE selectivity test graph a. MMIP-SPE-APTES and MNIP-SPE-APTES b. MMIP-SPE-OA and MNIP-SPE-OA.

4. Conclusion

In conclusion, we demonstrated at the computational stage a handy tool for rapidly selecting functional monomers and crosslinkers for template molecules in the synthesis of MMIPs and MIPs. Physical characteristic tests carried out using FT-IR, SEM-EDS, PSA, BET, and VSM showed that the synthesis was successful with a spherical and uniform agglomeration of particles. Also, a flat surface with many holes with a particle size of MMIP-APTES and MMIP-OA showed a surface area and exhibited superparamagnetic. MMIP-SPE-APTES meets the requirements for recovering analytes from biological samples, which is more than 80 %, and selective toward other compounds belonging to drugs.

Ethical statement

This study used blood plasma from Indonesian Red Cross as blank plasma without taking plasma directly by the researcher. No ethics approval needed for research purposes under Law Act of the Republic of Indonesia Number 1 of 2018 about Red Cross according to Law Act of the Republic of Indonesia Number 7 of 2011 concerning blood services.

Funding

This research has been supported by grants from Ministry of Education, Culture, Research and Technology Republic of Indonesia, Grants No. 1318/UN6.3.1/PT.00/2023.

Data availability statement

Data will be made available on request.

CRediT authorship contribution statement

Nur Masyithah Zamruddin: Writing – original draft, Investigation, Data curation. **Herman Herman:** Supervision, Conceptualization. **Saliza Asman:** Supervision, Conceptualization. **Aliya Nur Hasanah:** Writing – review & editing, Supervision, Funding acquisition, Conceptualization.

Declaration of competing interest

The authors declare the following financial interests/personal relationships which may be considered as potential competing interests:Aliya Nur Hasanah reports financial support was provided by Ministry of Education Culture Research and Technology. If there

are other authors, they declare that they have no known competing financial interests or personal relationships that could have appeared to influence the work reported in this paper.

References

[1] S. Wu, L. Lan, J. Jiang, X. Ding, C.M. Ho, Y. Lou, G. Fan, Simultaneous determination of the potent anti-tuberculosis regimen—pyrazinamide, ethambutol, protionamide, clofazimine in beagle dog plasma using LC–MS/MS method coupled with 96-well format plate, J. Pharm. Biomed. Anal. 168 (2019) 44–54, https://doi.org/10.1016/j.jpba.2019.02.006.

[2] Xu Jiabin, A. Koval, V Clofazimine Katanaev, A journey of a drug, Biomed & Pharmacoth 167 (2023) 1–12, https://doi.org/10.1016/j.biopha.2023.115539.

[3] F.M. Abdel-Haleem, E. Gamal, M.S. Rizk, A. Madbouly, R.M. El Nashar, B. Anis, H.M. Elnabawy, A.S.G. Khalil, A. Barhoum, Molecularly imprinted electrochemical sensor-based Fe2O3@MWCNTs for ivabradine drug determination in pharmaceutical formulation, serum, and urine samples, Front. Bioeng. Biotechnol. 9 (2021) 648704, https://doi.org/10.3389/fbioe.2021.648704.

[4] A.G. Märtson, G. Burch, S. Ghimire, J. Alfenaar, C. Peloquin, Therapeutic drug monitoring in patients with tuberculosis and concurrent medical problems, Expert Op on Drug Meta & Toxic 17 (2021) 23–39, https://doi.org/10.1080/17425255.2021.1836158.

[5] C. Magis-Escurra, J. van den Boogaard, D. Ijdema, M. Boeree, R. Aarnoutse, Therapeutic drug monitoring in the treatment of tuberculosis patients, Pulm. Pharmacol. Ther. 25 (2012) 83–86, https://doi.org/10.1016/j.pupt.2011.12.001.

[6] K.J. Seung, S. Keshavjee, M.L. Rich, Multidrug-resistant tuberculosis and extensively drug-resistant tuberculosis, Cold Spring Harb Perspect Med 5 (2015) a017863, https://doi.org/10.1101/cshperspect.a017863.

[7] M.T. Abdelwahab, S. Wasserman, J.C.M. Brust, N.R. Gandhi, G. Meintjes, D. Everitt, A. Diacon, R. Dawson, L. Wiesner, E.M. Svensson, et al., Clofazimine pharmacokinetics in patients with TB: dosing implications, J Antimicrobial Chem 75 (2020) 3269–3277, https://doi.org/10.1093/jac/dkaa310.

[8] C.H. Srikanth, P. Joshi, A.K. Bikkasani, K. Porwal, J.R. Gayen, Bone distribution study of anti leprotic drug clofazimine in rat bone marrow cells by a sensitive reverse phase liquid chromatography method, J. Chromatogr., B: Anal. Technol. Biomed. Life Sci. 960 (2014) 82–86, https://doi.org/10.1016/j.jchromb.2014.04.022.

[9] S. Wu, X. Fan, J. Jiang, C.M. Ho, X. Ding, Y. Lou, G. Fan, Validation of a universal and highly sensitive two-dimensional liquid chromatography–tandem mass spectrometry methodology for the quantification of pyrazinamide, ethambutol, protionamide, and clofazimine in different biological matrices, J. Chromatogr., B: Anal. Technol. Biomed. Life Sci. 1151 (2020) 122141, https://doi.org/10.1016/j.jchromb.2020.122141.

[10] S. Tyagi, N.C. Ammerman, S.Y. Li, J. Adamson, P.J. Converse, R.v. Swanson, D.v. Almeida, J.H. Grosset, Clofazimine shortens the duration of the first-line treatment regimen for experimental chemotherapy of tuberculosis, Proc Natl Acad Sci U S A 112 (2015) 869–874, https://doi.org/10.1073/pnas.1416951112.

[11] S. Machado, S.R. Fernandes, L.L. Chaves, S.A.C. Lima, E.M.P. Silva, L. Barreiros, S. Reis, M.A. Segundo, Chromatographic method for the simultaneous quantification of dapsone and clofazimine in nanoformulations, J Sep Sci 41 (2018) 3382–3388, https://doi.org/10.1002/jssc.201800427.

[12] J.L. Du Preez, M.E. Aucamp, C. Burger, M. Gerber, J.M. Viljoen, L. Van Zyl, J. Du Plessis, Development and validation of the simultaneous determination of artemisone, clofazimine and decoquinate with HPLC, Pharmazie 73 (2018) 139–142, https://doi.org/10.1691/ph.2018.7127.

[13] S. Ansari, M. Karimi, Recent configurations and progressive uses of magnetic molecularly imprinted polymers for drug analysis, Talanta 167 (2017) 470–485, https://doi.org/10.1016/j.talanta.2017.02.049.

[14] A.N. Hasanah, N. Safitri, A. Zulfa, N. Neli, D. Rahayu, Factors affecting preparation of molecularly imprinted polymer and methods on finding template-monomer interaction as the key of selective properties of the materials, Molecules 26 (2021) 5612, https://doi.org/10.3390/molecules26185612.

[15] G. Kojro, P. Wroczyński, Cloud point extraction in the determination of drugs in biological matrices, J. Chromatogr. Sci. 58 (2020) 151–162, https://doi.org/10.1093/chromsci/bmz064.

[16] I. Mohiuddin, S. Bhogal, A. Grover, A.K. Malik, J.S. Aulakh, Simultaneous determination of amitriptyline, nortriptyline, and clomipramine in aqueous samples using selective multi-template molecularly imprinted polymers, Environ. Nanotechnol. Monit. Manag. 16 (2021) 100527, https://doi.org/10.1016/j.enmm.2021.100527.

[17] A. Martín-Esteban, Molecularly-imprinted polymers as a versatile, highly selective tool in sample preparation, TrAC Trends Anal Chem 45 (2013) 169–181, https://doi.org/10.1016/j.trac.2012.09.023.

[18] F. Deng, X. Luo, L. Ding, S. Luo, Application of nanomaterials and nanotechnology in the reutilization of metal ion from wastewater, in: Nanomat for the Removal of Pollut and Res Reutiliz, 2018, pp. 149–178. ISBN 9780128148389.

[19] A. Karrat, J.M. Palacios-Santander, A. Amine, L. Cubillana-Aguilera, A novel magnetic molecularly imprinted polymer for selective extraction and determination of quercetin in plant samples, Anal. Chim. Acta 1203 (2022) 339709, https://doi.org/10.1016/j.aca.2022.339709.

[20] J. Giebultowicz, N. Korytowska, M. Sobiech, S. Polak, B. Wisniowska, R. Piotrowski, P. Kulakowski, P. Lulinski, Magnetic core-shell molecularly imprinted nano-conjugates for extraction of antazoline and hydroxyantazoline from human plasma-material characterization, theoretical analysis and pharmacokinetics, Int. J. Mol. Sci. 22 (2021) 3665, https://doi.org/10.3390/ijms22073665.

[21] M. Sobiech, J. Giebułtowicz, P. Luliński, Application of magnetic core-shell imprinted Nanoconjugates for the analysis of hordenine in human plasma-preliminary data on pharmacokinetic study after oral administration, J. Agric. Food Chem. 68 (2020) 14502–14512, https://doi.org/10.1021/acs.jafc.0c05985.

[22] S. Malik, A. Khan, G. Rahman, N. Ali, H. Khan, S. Khan, M.D.P.T. Sotomayor, Core-shell magnetic molecularly imprinted polymer for selective recognition and detection of sunset yellow in aqueous environment and real samples, Environ. Res. 212 (2022) 113209, https://doi.org/10.1016/j.envres.2022.113209.

[23] X. Wu, Y. Zhu, S. Bao, J. Cao, C. Zhao, X. Zhao, Z. Liu, X. Wang, Y. Fu, A novel and specific molecular imprinted polymer using cellulose as a carrier for the targeted separation of quercetin from Sophora japonica, Mater. Today Commun. 32 (2022) 104168, https://doi.org/10.1016/j.mtcomm.2022.104168.

[24] W. Ji, R. Sun, W. Duan, X. Wang, T. Wang, Y. Mu, L. Guo, Selective solid phase extraction of chloroacetamide herbicides from environmental water samples by amphiphilic magnetic molecularly imprinted polymers, Talanta 170 (2017) 111–118, https://doi.org/10.1016/j.talanta.2017.04.005.

[25] N. Laskar, D. Ghoshal, S. Gupta, Chitosan-based magnetic molecularly imprinted polymer: synthesis and application in selective recognition of tricyclazole from rice and water samples, Iranian Pol J (English Edition) 30 (2021) 121–134, https://doi.org/10.1007/s13726-020-00878-6.

[26] T. Kubo, K. Otsuka, Recent progress in molecularly imprinted media by new preparation concepts and methodological approaches for selective separation of targeting compounds, TrAC Trends in Anal Chem 81 (2016) 102–109, https://doi.org/10.1016/j.trac.2015.08.008.

[27] S. Huang, J. Xu, J. Zheng, F. Zhu, L. Xie, G. Ouyang, Synthesis and application of magnetic molecularly imprinted polymers in sample preparation, Anal. Bioanal. Chem. 410 (2018) 3991–4014, https://doi.org/10.1007/s00216-018-1013-y.

[28] M. Woźnica, M. Sobiech, P. Luliński, A fusion of molecular imprinting Technology and siloxane chemistry: a way to advanced hybrid nanomaterials, Nanomaterials 13 (2023) 248, https://doi.org/10.3390/nano13020248.

[29] C. Lafarge, M. Bitar, L. El Hosry, P. Cayot, E. Bou-Maroun, Comparison of molecularly imprinted polymers (MIP) and sol–gel molecularly imprinted silica (MIS) for fungicide in a hydro alcoholic solution, Mater. Today Commun. 24 (2020) 101157, https://doi.org/10.1016/j.mtcomm.2020.101157.

[30] S. Suryana, M. Mutakin, Y. Rosandi, A.N. Hasanah, Rational design of salmeterol xinafoate imprinted polymer through computational method: functional monomer and crosslinker selection, Polym. Adv. Technol. 33 (2021) 221–234, https://doi.org/10.1002/pat.5507.

[31] S. Suryana, Mutakin, Y. Rosandi, A.N. Hasanah, An update on molecularly imprinted polymer design through a computational approach to produce molecular recognition material with enhanced analytical performance, Molecules 26 (2021) 1891, https://doi.org/10.3390/molecules26071891.

[32] L. Chen, B. Li, Magnetic molecularly imprinted polymer extraction of chloramphenicol from honey, Food Chem. 141 (2013) 23–28, https://doi.org/10.1016/j.foodchem.2013.02.085.

[33] N.R. Jannah, D. Onggo, Synthesis of Fe3O4 nanoparticles for colour removal of printing ink solution, J Physics: Conference Series 1245 (2019) 012040, https://doi.org/10.1088/1742-6596/1245/1/012040.

[34] M. Mehdipour, M. Ansari, M. Pournamdari, L. Zeidabadinejad, M. Kazemipour, Selective extraction of organophosphorous pesticides in plasma by magnetic molecularly imprinted polymers with the aid of computational design, Anal. Methods 10 (2018) 4136–4142, https://doi.org/10.1039/c8ay00955d.

[35] M. Ali Zulfikar, A. Rizqi Utami, N. Handayani, D. Wahyuningrum, H. Setiyanto, M. Yudhistira Azis, Removal of phthalate ester compound from PVC plastic samples using magnetic molecularly imprinted polymer on the surface of superparamagnetic Fe3O4 (Fe3O4@MIPs), Environ. Nanotechnol. Monit. Manag. 17 (2022) 100646, https://doi.org/10.1016/j.enmm.2022.100646.
[36] S. Azodi-Deilami, A.H. Najafabadi, E. Asadi, M. Abdouss, D. Kordestani, Magnetic molecularly imprinted polymer nanoparticles for the solid-phase extraction of paracetamol from plasma samples, followed its determination by HPLC, Microchim. Acta 181 (2014) 1823–1832, https://doi.org/10.1007/s00604-014-1230-9.
[37] A.N. Hasanah, D. Fauzi, B.Z. Witka, D. Rahayu, R. Pratiwi, Molecular imprinted polymer for ethylmorphine with methacrylic acid and acrylamide as functional monomer in butanol using two polymerization method, Mediterranean Journal of Chemistry 10 (2020) 277–288, https://doi.org/10.13171/mjc02003211282anh.
[38] H. Krishnan, K. Islam, Z. Hamzah, M. Ahmad, Rational computational design for the development of andrographolide molecularly, AIP Confer Proceed 1891 (2017) 1–8, https://doi.org/10.1063/1.5005416.
[39] N. Reyes, B. Pajarito, Computational design of dummy molecularly imprinted polymers via hydrogen bonding investigation for oxytetracycline determination, IOP Conferen Ser: Mat Sci and Engine 634 (2019) 1–8, https://doi.org/10.1088/1757-899X/634/1/012035.
[40] G. Gelardi, R.J. Flatt, Working mechanisms of water reducers and superplasticizers, in: Science and Technology of Concrete Admixtures, Elsevier Inc., 2016, pp. 257–278. ISBN 9780081006962.
[41] L. Chen, S. Xu, J. Li, Recent advances in molecular imprinting Technology: current status, challenges and highlighted applications, Chem. Soc. Rev. 40 (2011) 2922–2942, https://doi.org/10.1039/c0cs00084a.
[42] K. Kirimura, Y. Honda, T. Hattori, 3.14 - Gluconic and Itaconic Acids. In Compre Biotech (Second Edition) ; Tokyo, Japan 3 (2011) 143–147.
[43] M.P. Pešić, M.D. Todorov, G. Becskereki, G. Horvai, T. Verbić, B. Tóth, A novel method of molecular imprinting applied to the template cholesterol, Talanta 217 (2020) 121075, https://doi.org/10.1016/j.talanta.2020.121075.
[44] P. Luliński, D. Maciejewska, Examination of imprinting process with molsidomine as a template, Molecules 14 (2009) 2212–2225, https://doi.org/10.3390/molecules14062212.
[45] N.A. Hasanah, R. Pratiwi, T. Rostinawati, S. Megantara, S. Amelia, Febrina, P. Hidayati, H. Khanifa, Extraction of atenolol from spiked blood serum using a molecularly imprinted polymer sorbent obtained by precipitation polymerization, Heliyon 5 (2019) e01533, https://doi.org/10.1016/j.heliyon.2019.
[46] Y.Q. Zhang, P.L. Yu, W.F. Sun, X. Wang, Ameliorated electrical-tree resistant characteristics of uv-initiated cross-linked polyethylene nanocomposites with surface-functionalized nanosilica, Processes 9 (2021) 313, https://doi.org/10.3390/pr9020313.
[47] L. Nalbandian, E. Patrikiadou, V. Zaspalis, A. Patrikidou, E. Hatzidaki, C. N. Papandreou, Magnetic nanoparticles in medical diagnostic applications: synthesis, characterization and proteins conjugation, Curr. Nanosci. 12 (2015) 455–468, https://doi.org/10.2174/1573413712666151210230002.
[48] A.K. Bordbar, A.A. Rastegari, R. Amiri, E. Ranjbakhsh, M. Abbasi, A.R. Khosropour, Characterization of modified magnetite nanoparticles for albumin immobilization, Biotechnol Res Int 2014 (2014) 1–6, https://doi.org/10.1155/2014/705068.
[49] L.L. Chaves, S. Lima, A.C.C. Vieira, D. Ferreira, B. Sarmento, S. Reis, Overcoming clofazimine intrinsic toxicity: statistical modelling and characterization of solid lipid nanoparticles, J R Soc Interface 15 (2018), https://doi.org/10.1098/rsif.2017.0932.
[50] B.P.H. Do, B.D. Nguyen, H.D. Nguyen, P.T. Nguyen, Synthesis of magnetic composite nanoparticles enveloped in copolymers specified for scale inhibition application, Adv. Nat. Sci. Nanosci. Nanotechnol. 4 (2013), https://doi.org/10.1088/2043-6262/4/4/045016.
[51] E. Alzahrani, Photodegradation of binary azo dyes using core-shell Fe3O4/SiO2/TiO2 nanospheres, American J Anal Chem 8 (2017) 95–115, https://doi.org/10.4236/ajac.2017.81008.
[52] S.S. Alterary, A. Synthesis Alkhamees, Surface modification, and characterization of Fe3O4@SiO2core@shell nanostructure, Green Process. Synth. 10 (2021) 384–391, https://doi.org/10.1515/gps-2021-0031.
[53] L. Yi, R. Fang, G. Chen, Molecularly imprinted solid-phase extraction in the analysis of agrochemicals, J. Chromatogr. Sci. 51 (2013) 608–618, https://doi.org/10.1093/chromsci/bmt024.
[54] N. Zamruddin, H. Herman, L. Rijai, A. Hasanah, Factors affecting the analytical performance of magnetic molecularly imprinted polymers, Polymer (Guildf) 14 (2022) 1–25, https://doi.org/10.3390/polym14153008.
[55] H.W. Mukami, B.S. Batlokwa, Application of a custom-synthesized molecularly imprinted polymer for the selective isolation of total glucose and fructose from 100% fruit juice samples prior to instrumental analysis, Molecular Imprinting 5 (2018) 16–24, https://doi.org/10.1515/molim-2018-0001.
[56] M.G.F. Stevens, B.S. Batlokwa, Multi-templated Pb-Zn-Hg ion imprinted polymer for the selective and simultaneous removal of toxic metallic ions from wastewater, Int. J. Chem. 9 (2017) 10–22, https://doi.org/10.5539/ijc.v9n2p10.
[57] Y. Cao, Z. Huang, L. Luo, J. Li, P. Li, X. Liu, Rapid and selective extraction of norfloxacin from milk using magnetic molecular imprinting polymers nanoparticles, Food Chem. 353 (2021) 129464, https://doi.org/10.1016/j.foodchem.2021.129464.
[58] C. Cao, L. Xiao, C. Chen, X. Shi, Q. Cao, L. Gao, In situ preparation of magnetic Fe3O4/chitosan nanoparticles via a novel reduction-precipitation method and their application in adsorption of reactive azo dye, Powder Technol. 260 (2014) 90–97, https://doi.org/10.1016/j.powtec.2014.03.025.
[59] M. Padma Sree, Vibrating sample magnetometer and its application in characterisation of magnetic property of the anti cancer drug magnetic microspheres, International Journal of Pharmaceutics & Drug Analysis 4 (2016) 227–233.
[60] M. Sobiech, K. Synoradzki, T.J. Bednarchuk, K. Sobczak, M. Janczura, J. Giebułtowicz, P. Luliński, Impact of structure and magnetic parameters of nanocrystalline cores on surface properties of molecularly imprinted Nanoconjugates for analysis of biomolecules – a case of tyramine, Microchem. J. 179 (2022) 107571, https://doi.org/10.1016/j.microc.2022.107571.
[61] A.N. Hasanah, D. Soni, R. Pratiwi, D. Rahayu, S. Megantara, Mutakin synthesis of diazepam-imprinted polymers with two functional monomers in chloroform using a bulk polymerization method, J. Chem. 2020 (2020), https://doi.org/10.1155/2020/7282415.
[62] V. Kumar, G. Srinivas, B. Wood, K.K. Ramisetty, Supplementary for "characterization of adsorption site energies and heterogeneous surfaces of porous materials.", J. Mater. Chem. A 7 (2019) 10104–10137, https://doi.org/10.1039/C9TA00287A.
[63] V.K.S. Hsiao, J.R. Waldeisen, Y. Zheng, P.F. Lloyd, T.J. Bunning, T.J. Huang, Aminopropyltriethoxysilane (APTES)-Functionalized nanoporous polymeric gratings: fabrication and application in biosensing, J. Mater. Chem. 17 (2007) 4896–4901, https://doi.org/10.1039/b711200a.
[64] L. Zhang, R. He, H.C. Gu, Oleic acid coating on the monodisperse magnetite nanoparticles, Appl. Surf. Sci. 253 (2006) 2611–2617, https://doi.org/10.1016/j.apsusc.2006.05.023.